USGS
science for a changing world

System Characterization Report on Resourcesat-2A Advanced Wide Field Sensor

Chapter V of
System Characterization of Earth Observation Sensors

Open-File Report 2021–1030–V

U.S. Department of the Interior
U.S. Geological Survey

System Characterization Report on Resourcesat-2A Advanced Wide Field Sensor

By Mahesh Shrestha,[1] Minsu Kim,[1] Aparajithan Sampath,[1] and Jeffrey Clausen[2]

Chapter V of

System Characterization of Earth Observation Sensors

Compiled by Shankar N. Ramaseri Chandra[1]

[1]KBR, Inc., under contract to the U.S. Geological Survey.

[2]U.S. Geological Survey.

Open-File Report 2021–1030–V

U.S. Department of the Interior
U.S. Geological Survey

U.S. Geological Survey, Reston, Virginia: 2025

Suggested citation:
Shrestha, M., Kim, M., Sampath, A., and Clausen, J., 2025, System characterization report on Resourcesat-2A Advanced Wide Field Sensor, chap. V *of* Ramaseri Chandra, S.N., comp., System characterization of Earth observation sensors: U.S. Geological Survey Open-File Report 2021–1030, 18 p., https://doi.org/10.3133/ofr20211030V.

ISSN 2331-1258 (online)

Contents

Figures

Tables

Conversion Factors

International System of Units to U.S. customary units

Multiply	By	To obtain
	Length	
meter (m)	3.281	foot (ft)
meter (m)	1.094	yard (yd)
kilometer (km)	0.6214	mile (mi)

Abbreviations

AWiFS	Advanced Wide Field Sensor
ECCOE	EROS Cal/Val Center of Excellence
EROS	Earth Resources Observation and Science
EROSSC	EROS System Characterization
GSD	ground sample distance
JACIE	Joint Agency Commercial Imagery Evaluation
OLI	Operational Land Imager
PICS	pseudoinvariant calibration sites
RadCalNet	Radiometric Calibration Network
RMSE	root mean square error
SBAF	spectral band adjustment factor
TOA	Top of Atmosphere
USGS	U.S. Geological Survey

System Characterization Report on Resourcesat-2A Advanced Wide Field Sensor

By Mahesh Shrestha,[1] Minsu Kim,[1] Aparajithan Sampath,[1] and Jeffrey Clausen[2]

Executive Summary

This report documents the system characterization of the Indian Space Research Organisation Resourcesat-2A (Indian Space Research Organisation, 2023) Advanced Wide Field Sensor (AWiFS) and is part of a series of system characterization reports produced by the U.S. Geological Survey Earth Resources Observation and Science Cal/Val Center of Excellence (U.S. Geological Survey, 2021). These reports describe the methodology and procedures used for characterization, present technical and operational information about the specific sensing system being evaluated, and provide a summary of test measurements, data retention practices, data analysis results, and conclusions.

Resourcesat-2A was launched in 2016 on the Polar Satellite Launch Vehicle-C36; it is identical to Resourcesat-2, and together, they decrease imaging revisit time from 5 days to 2–3 days, providing data continuity and improved temporal resolution. Resourcesat-2 and -2A carry the AWiFS, Linear Imaging Self Scanning-3, and Linear Imaging Self Scanning-4 medium-resolution imaging sensors, continuing the legacy of the Indian Space Research Organisation's Indian Remote Sensing-1C/1D/P3 satellite programs. More information about Indian Space Research Organisation satellites and sensors is available through the Joint Agency Commercial Imagery Evaluation Earth Observing Satellites Online Compendium (Clauson and others, 2024) and from the Indian Space Research Organisation at https://www.isro.gov.in/.

The Earth Resources Observation and Science Cal/Val Center of Excellence system characterization team assessed the geometric, radiometric, and spatial performance of the Resourcesat-2A AWiFS sensor. Geometric performance is divided into the interior geometric performance of band-to-band registration and the exterior geometric performance of geolocation accuracy. The interior geometric performance had offsets in the range of −1.10 meters (m; −0.020 pixel) to 3.67 m (0.066 pixel) in easting and −5.68 m (−0.101 pixel) to 10.38 m (0.185 pixel) in northing with root mean square error values from 5.60 m (0.100 pixel) to 11.31 m (0.202 pixel) in easting and from 3.00 m (0.054 pixel) to 13.52 m (0.241 pixel) in northing.

The exterior geometric performance had mean offsets of −25.29 m in easting and 16.22 m northing with root mean square error values of 26.07 m in easting and 17.60 m in northing compared to the Landsat 8 Operational Land Imager sensor (Earth Resources Observation and Science Center, 2020). The radiometric performance had offsets from −0.002 to 0.029 and slopes from 0.733 to 1.012. Spatial performance was in the range of 1.354 to 1.639 pixels for full width at half maximum with a modulation transfer function at a Nyquist frequency in the range of 0.108 to 0.174.

References Cited

Clauson, J., Cantrell, S., Vrabel, J., Oeding, J., Ranjitkar, B., Rusten, T., Ramaseri, S., and Casey, K., 2024, Earth observing sensing satellites online compendium: U.S. Geological Survey digital data, accessed March 7, 2025, at https://calval.cr.usgs.gov/apps/compendium.

Earth Resources Observation and Science Center, 2020, Landsat 8–9 Operational Land Imager/Thermal Infrared Sensor Level-1, Collection 2: U.S. Geological Survey digital data, accessed April 16, 2025, at https://doi.org/10.5066/P975CC9B.

Indian Space Research Organisation, 2023, Resourcesat-2A: Indian Space Research Organisation web page, accessed August 30, 2024, at https://www.isro.gov.in/RESOURCESAT_2A.html.

U.S. Geological Survey, 2021, EROS CalVal Center of Excellence (ECCOE): U.S. Geological Survey web page, accessed October 2024 at https://www.usgs.gov/calval.

[1]KBR, Inc., under contract to the U.S. Geological Survey.

[2]U.S. Geological Survey.

Introduction

This report documents the system characterization of the Indian Space Research Organisation Resourcesat-2A (Indian Space Research Organisation, 2023) Advanced Wide Field Sensor (AWiFS) and is part of a series of system characterization reports produced by the U.S. Geological Survey (USGS) Earth Resources Observation and Science (EROS) Cal/Val Center of Excellence (ECCOE; U.S. Geological Survey, 2021a). These reports describe the methodology and procedures used for characterization, present technical and operational information about the specific sensing system being evaluated, and provide a summary of test measurements, data retention practices, data analysis results, and conclusions.

The Resourcesat-2A AWiFS is a wide-angle medium-resolution camera consisting of four bands: green, red, near infrared, and shortwave infrared (Indian Space Research Organisation, 2023). The camera has a swath width of 740 kilometers, enabling AWiFS to provide a 5-day repeat capability. The primary objectives for data acquired by AWiFS include vegetation and crop monitoring, forest mapping, land cover/land use mapping, change detection, and regional resource assessment.

The data analysis results provided in this report have been derived from Joint Agency Commercial Imagery Evaluation (JACIE) processes and procedures. JACIE was formed to leverage resources from several Federal agencies for the characterization of remote sensing data and to share those results across the remote sensing community (U.S. Geological Survey, 2021b).

Purpose and Scope

The purpose of this report is to describe the specific sensor or sensing system, test its performance in three categories, complete related data analyses to quantify these performances, and report the results in a standardized document. In this chapter, the AWiFS sensor is described. The performance assessment of the system is limited to geometric, radiometric, and spatial analyses. The scope of the geometric assessment is limited to testing the interior alignments of spectral bands against each other and testing the exterior alignment in reference to the Landsat 8 Operational Land Imager (OLI; Earth Resources Observation and Science Center, 2020; U.S. Geological Survey, 2021c).

The system characterization process used by the ECCOE team (U.S. Geological Survey, 2021a) follows the USGS Fundamental Science Practices, which include maintaining data, information, and documentation needed to reproduce and validate the scientific analysis documented in this report. Additional information and guidance about Fundamental Science Practices are available at https://www.usgs.gov/office-of-science-quality-and-integrity/fundamental-science-practices. For additional information related to the report, please contact ECCOE at eccoe@usgs.gov.

System Description

This section describes the satellite and operational details for Resourcesat-2A and provides information about the AWiFS sensor. Resourcesat-2A was launched in 2016 on the Polar Satellite Launch Vehicle-C36; it is identical to Resourcesat-2, and together, they decrease imaging revisit time from 5 days to 2–3 days, providing data continuity and improved temporal resolution. Resourcesat-2 and -2A carry the AWiFS, Linear Imaging Self Scanning-3, and Linear Imaging Self Scanning-4 medium-resolution imaging sensors, continuing the legacy of the Indian Space Research Organisation's Indian Remote Sensing-1C/1D/P3 satellite programs. More information about Indian Space Research Organisation satellites and sensors is available through the Joint Agency Commercial Imagery Evaluation Earth Observing Satellites Online Compendium (Clauson and others, 2024) and from the Indian Space Research Organisation at https://www.isro.gov.in/.

Satellite and Operational Details

The satellite and operational details of Resourcesat-2A and information about the AWiFS are listed in table 1.

Sensor Information

The spectral characteristics and the relative spectral response of the AWiFS are listed in table 2 and shown in figure 1, respectively.

Table 1. Satellite and operational details for Resourcesat-2A Advanced Wide Field Sensor (Indian Space Research Organisation, 2023).

[kg, kilogram; NIR, near infrared; SWIR, shortwave infrared; W, watt; AH, amp hour; Ni-Cd, nickel-cadmium; Mbps, megabit per second; ~, about; km, kilometer; °, degree; min, minute; ±, plus or minus; lat., latitude; NA, not applicable; m, meter]

Product information	Resourcesat-2A Advanced Wide Field Sensor data
Satellite and operational information	
Product name	Level 1T
Satellite name	Resourcesat-2A
Sensor name	Advanced Wide Field Sensor
Lift-off mass	1,235 kg
Instrument mass	106 kg
Sensor type	Multispectral, visible, and infrared (green, red, NIR, SWIR)
Scanning technique	Pushbroom; 6,000 detectors array
Power	Solar array generating 1,250 W at end of life; two 24 AH Ni-Cd batteries
Data rate	52.5 Mbps
Mission type	Global land-monitoring mission
Launch date	December 7, 2016
Number of satellites	1
Expected lifetime	~5 years
Operator	Indian Space Research Organisation
Operational details	
Operating orbit	Circular polar Sun synchronous
Orbital altitude range	817 km
Sensor angle altitude	98.7° inclination
Altitude and orbit control	Three-axis body stabilized using reaction wheels, magnetic torquers, and hydrazine thrusters
Orbit period	101.35 min
Imaging time	10:30 descending node
Geographic coverage	Land imaging ±81.3° lat.
Temporal resolution	24 days
Temporal coverage	2016 to present (2025)
Imaging angles	NA
Ground sample distance(s)	56 m
Data licensing	NA
Data pricing	NA
Product abstract	Resourcesat-2A (https://www.isro.gov.in/)
Product locator	NA

Table 2. Imaging sensor details for Resourcesat-2A Advanced Wide Field Sensor (Indian Space Research Organisation, 2023).

[The Resourcesat-2A Advanced Wide Field Sensor (AWiFS) has a swath width of 740 kilometers; µm, micrometer; m, meter; NIR, near infrared; SWIR, shortwave infrared]

Spectral band(s) details	Resourcesat-2A AWiFS			
	Lower band (µm)	Upper band (µm)	Radiometric resolution (bits)	Ground sample distance (m)
Band 2—green	0.52	0.59	10	56
Band 3—red	0.62	0.68	10	56
Band 4—NIR	0.77	0.86	10	56
Band 5—SWIR	1.55	1.70	10	56

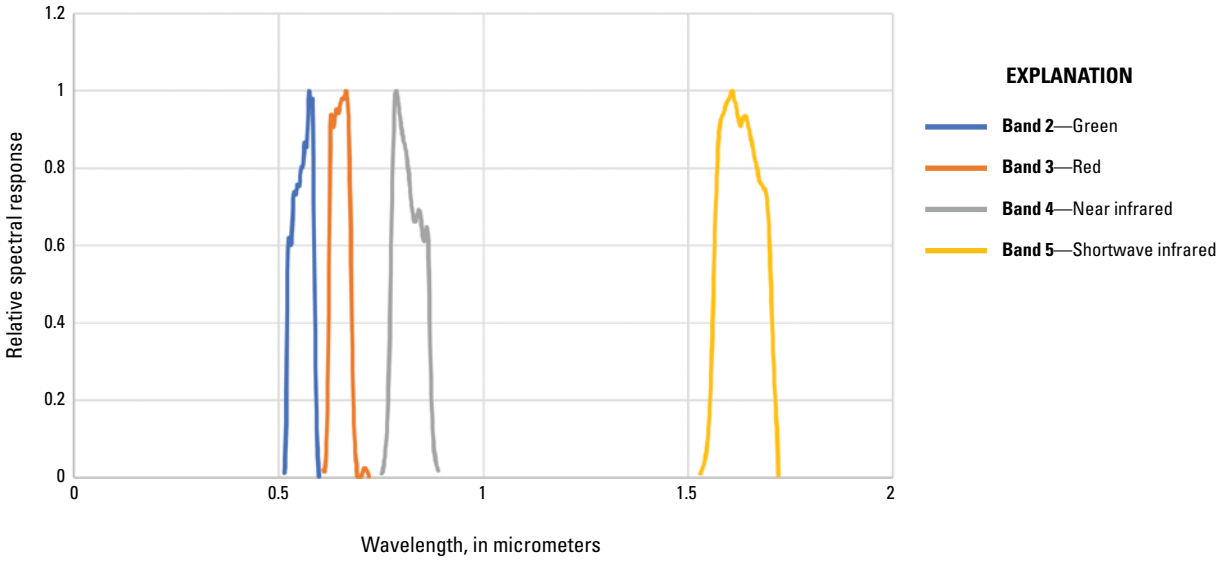

Figure 1. Graph showing Resourcesat-2A Advanced Wide Field Sensor relative spectral response (Indian Space Research Organisation, 2023).

Procedures

ECCOE has established standard processes to identify Earth observing systems of interest and to assess the geometric, radiometric, and spatial qualities of data products from these systems.

The assessment steps are as follows:

- system identification and investigation to learn the general specifications of the satellite and its sensor(s);
- data receipt and initial inspection to understand the characteristics and any overt flaws in the data product so that it may be further analyzed;
- geometry characterization, including interior geometric orientation measuring the relative alignment of spectral bands and exterior geometric orientation measuring how well the georeferenced pixels within the image are aligned to a known reference;
- radiometry characterization, including assessing how well the data product correlates with a known reference and, when possible, assessing the signal-to-noise ratio; and
- spatial characterization, assessing the two-dimensional fidelity of the image pixels to their projected ground sample distance (GSD).

Data analysis and test results are maintained at the USGS EROS Center by the ECCOE project.

Measurements

The observed USGS measurements are listed in table 3. The mean error and root mean square error (RMSE) values for interior (band-to-band) and exterior (image-to-image) geometric performance are listed in meters (pixels). These values are derived from tables 4, 5, 6, and 7 and are summarized here. The values for interior and exterior geometry and for radiometry are the averages of three datasets used for the analysis. The spatial performance is assessed on a single scene and is reported without averages. Details about the methodologies used are outlined in the "Analysis" section.

Table 3. U.S. Geological Survey measurement results.

[m, meter; RMSE, root mean square error; NIR, near infrared; SWIR, shortwave infrared; AWiFS, Advanced Wide Field Sensor; L8 OLI, Landsat 8 Operational Land Imager; FWHM, full width at half maximum; MTF, modulation transfer function]

Description of product	Top of Atmosphere reflectance
Geometric performance (easting, northing), in meters (pixels)	
Interior (band to band where reference band is band 2 [green]) averages	Band 3 (red) Mean: 3.67 m (0.066), 0.97 m (0.100) RMSE: 5.62 m (0.100), 3.00 m (0.054) Band 4 (NIR) Mean: 0.86 m (0.015), 10.38 m (0.185) RMSE: 11.31 m (0.202), 13.52 m (0.241) Band 5 (SWIR) Mean: −1.10 m (−0.020), −5.68 m (−0.101) RMSE: 5.60 m (0.100), 7.11 m (0.127)
Exterior (geometric location accuracy)	Mean: −25.29 m (−0.45), 16.22 m (0.289) RMSE: 26.07 m (0.465), 17.60 m (0.314)
Radiometric performance (offset, slope)	
Radiometric evaluation (linear regression—AWiFS versus L8 OLI[1] reflectance)	Band 2—Green (offset, slope): (0.009, 0.909) Band 3—Red (offset, slope): (0.019, 0.842) Band 4—NIR (offset, slope): (0.029, 0.733) Band 5—SWIR (offset, slope): (−0.002, 1.012)
Spatial performance	
Spatial performance measurement	Band 2—Green: FWHM=1.430 pixels; MTF at Nyquist=0.174 Band 3—Red: FWHM=1.354 pixels; MTF at Nyquist=0.154 Band 4—NIR: FWHM=1.547 pixels; MTF at Nyquist=0.148 Band 5—SWIR: FWHM=1.639 pixels; MTF at Nyquist=0.108

[1]Earth Resources Observation and Science Center (2020).

Table 4. Band-to-band registration error of Resourcesat-2A Advanced Wide Field Sensor (Indian Space Research Organisation, 2023) relative to Landsat 8 Operational Land Imager (Earth Resources Observation and Science Center, 2020) in pixels resampled to a 60-meter ground sample distance.

[ID, identifier; RMSE, root mean square error]

Scene ID	Band combination	Mean error (easting)	Mean error (northing)	RMSE (easting)	RMSE (northing)
R2A_AW__27-MAY-2023_100_061_GEOREF	Band 2–band 3	0.065	0.018	0.081	0.032
	Band 2–band 4	0.018	0.221	0.134	0.24
	Band 2–band 5	−0.019	−0.095	0.075	0.105
R2A_AW__11-NOV-2023_100_063_GEOREF	Band 2–band 3	0.07	0.011	0.093	0.045
	Band 2–band 4	−0.039	0.18	0.26	0.278
	Band 2–band 5	−0.038	−0.069	0.087	0.092
R2A_AW__29-JUL-2023_252_045_GEOREF	Band 2–band 3	0.062	0.023	0.127	0.084
	Band 2–band 4	0.067	0.155	0.213	0.206
	Band 2–band 5	−0.002	−0.138	0.138	0.184

Table 5. Geometric error of Resourcesat-2A Advanced Wide Field Sensor (Indian Space Research Organisation, 2023) relative to Landsat 8 Operational Land Imager (Earth Resources Observation and Science Center, 2020) in meters at a 60-meter ground sample distance.

[ID, identifier; RMSE, root mean square error]

Scene ID	Mean error (easting)	Mean error (northing)	RMSE error (easting)	RMSE error (northing)
239329711_R2A_AW__27-MAY-2023_100_061_GEOREF	−20.30 m	21.37 m	22.08 m	22.08 m
239329911_R2A_AW__11-NOV-2023_100_063_GEOREF	−25.47 m	11.05 m	25.82 m	11.81 m
239330611_R2A_AW__10-JUN-2023_026_032_GEOREF	−30.08 m	16.23 m	30.31 m	18.91 m

Table 6. Top of Atmosphere reflectance comparison of Resourcesat-2A Advanced Wide Field Sensor (Indian Space Research Organisation, 2023) against Landsat 8 Operational Land Imager (Earth Resources Observation and Science Center, 2020) over Railroad Valley playa, Nevada.

[ID, identifier; B, band; %, percent; R^2, coefficient of determination]

Scene IDs (Advanced Wide Field Sensor versus Landsat 8 Operational Land Imager)	Statistics	Band 2	Band 3	Band 4	Band 5
239329711_R2A_AW__27-MAY-2023_100_061_GEOREF versus LC08_L1TP_144048_20230527_20230603_02_T1	Uncertainty (%)	6.322	9.616	9.475	8.981
	R^2	0.853	0.854	0.867	0.916
	Radical offset	0.009	0.024	0.034	0.016
	Radical slope	0.938	0.833	0.713	0.981
239329911_R2A_AW__11-NOV-2023_100_063_GEOREF versus LC09_L1TP_144049_20231111_20231111_02_T1	Uncertainty (%)	5.561	10.9	7.397	9.443
	R^2	0.919	0.922	0.905	0.934
	Radical offset	0.004	0.01	0.013	−0.02
	Radical slope	0.906	0.854	0.786	1.023
239330611_R2A_AW__10-JUN-2023_026_032_GEOREF versus LC08_L1TP_194024_20230610_20230614_02_T1	Uncertainty (%)	6.528	10.774	9.909	11.707
	R^2	0.785	0.826	0.784	0.862
	Radical offset	0.015	0.023	0.039	−0.002
	Radical slope	0.884	0.838	0.7	1.032

Table 7. Radiometric analyses by estimating spectral band adjustment factors between Landsats 8 and 9 Operational Land Imager (Earth Resources Observation and Science Center, 2020) and Advanced Wide Field Sensor using Resourcesat-2A Advanced Wide Field Sensor (Indian Space Research Organisation, 2023).

[RadCalNet data from Bouvet and others (2019). ID, identifier; NIR, near infrared; SWIR, shortwave infrared; RadCalNet, Radiometric Calibration Network; OLI, Operational Land Imager]

Scene ID	Reference	Region of interest	Spectral band adjustment factor			
			Green	Red	NIR	SWIR
239330721_R2A_AW__29-JUL-2023_252_045_GEOREF	RadCalNet	Railroad Valley playa[1]	0.987	0.966	0.960	1.006
239330711_R2A_AW__15-SEP-2023_252_045_GEOREF	RadCalNet	Railroad Valley playa[1]	0.921	0.894	0.878	0.943
239330721_R2A_AW__29-JUL-2023_252_045_GEOREF	Landsat 9 OLI	Railroad Valley playa[1]	1.044	1.002	0.986	1.003
239330711_R2A_AW__15-SEP-2023_252_045_GEOREF	Landsat 9 OLI	Railroad Valley playa[1]	0.901	0.865	0.842	0.892
239321611_R2A_AW__04-AUG-2023_037_055_GEOREF	Landsat 9 OLI	[2]Libya 1	1.036	0.975	0.955	0.918
239321621_R2A_AW__21-SEP-2023_037_055_GEOREF	Landsat 9 OLI	[2]Libya 1	1.043	0.984	0.965	0.928
239329621_R2A_AW__10-JUN-2023_026_047_GEOREF	Landsat 9 OLI	[3]Algeria 5	1.003	0.927	0.904	0.887
239329611_R2A_AW__09-JUL-2023_027_048_GEOREF	Landsat 8 OLI	[3]Algeria 5	1.099	1.013	0.989	0.956
239329631_R2A_AW__28-JUL-2023_026_047_GEOREF	Landsat 9 OLI	[3]Algeria 5	1.045	0.976	0.976	0.945
239329621_R2A_AW__10-JUN-2023_026_047_GEOREF	Landsat 9 OLI	[3]Algeria 5	1.065	0.993	0.999	0.956
239329611_R2A_AW__09-JUL-2023_027_048_GEOREF	Landsat 9 OLI	[3]Algeria 5	1.098	1.022	1.016	0.954
239329631_R2A_AW__28-JUL-2023_026_047_GEOREF	Landsat 9 OLI	[3]Algeria 5	1.066	0.99	1.001	0.949

[1]The region of interest is in Railroad Valley playa, Nevada.

[2]The region of interest is in the Sahara Desert in Libya.

[3]The region of interest is in the Grand Erg Occidental in Algeria.

Analysis

This section describes the geometric, radiometric, and spatial performance of AWiFS.

Geometric Performance

The geometric performance for AWiFS is characterized in terms of the interior (band-to-band alignment) and exterior (geometric location accuracy) geometric analysis results.

Interior (Band to Band)

The band-to-band alignment analysis was completed using the EROS System Characterization (EROSSC) software (Cantrell and Christopherson, 2024) on three separate images. Band combinations were registered against each other to determine the mean error and RMSE values as listed in table 4 with results represented in pixels resampled to a 60-meter (m) GSD from the original 56-m GSD. Example error scatterplots and histograms for scene identifier 239329911_R2A_AW__11-NOV-2023_100_063_GEOREF (Indian Space Research Organisation, 2023) are shown in figures 2, 3, and 4.

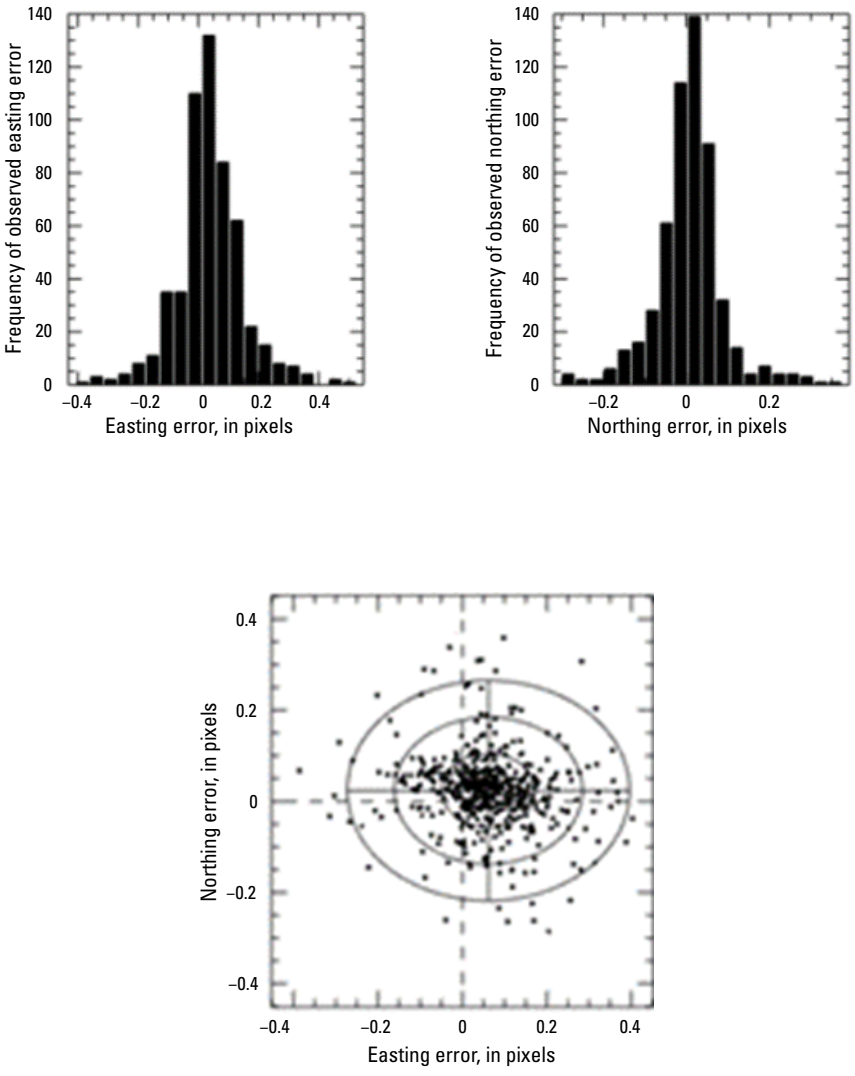

Figure 2. Band 2 (green) to band 3 (red) geometric error histogram (upper) and error distribution (lower) (scene identifier 239329911_R2A_AW__11-NOV-2023_100_063_GEOREF).

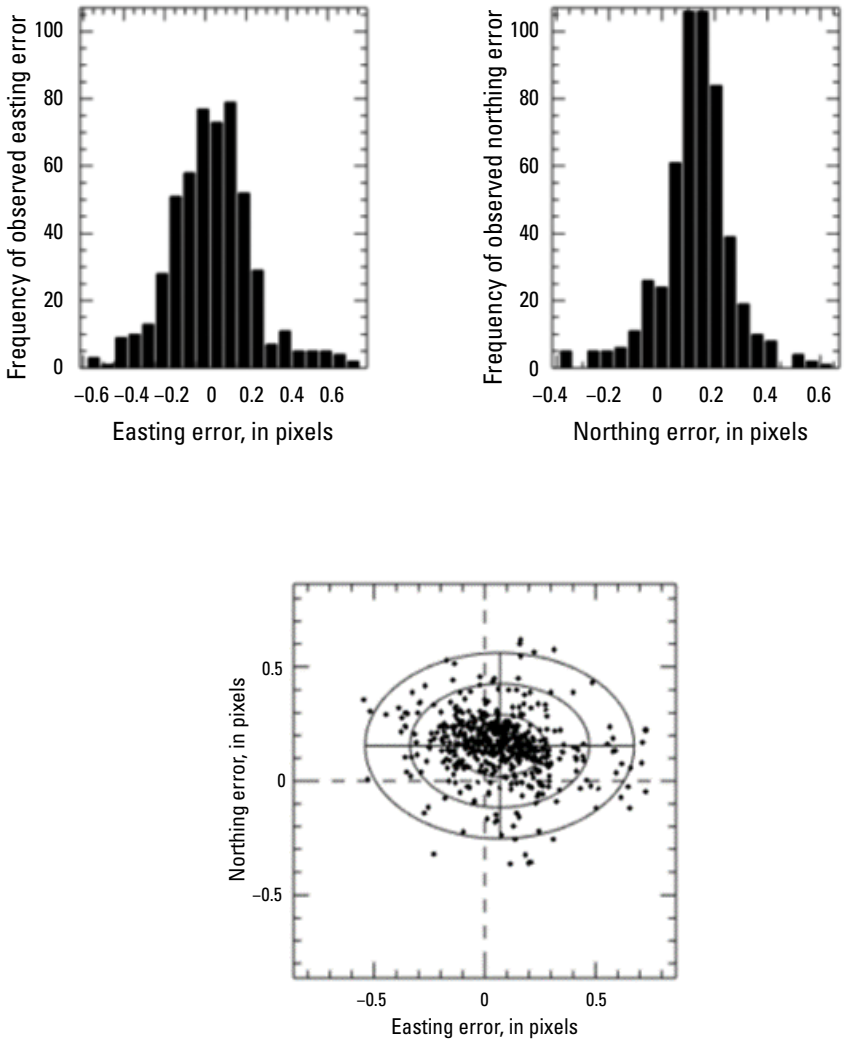

Figure 3. Band 3 (green) to band 4 (near infrared) geometric error histogram (upper) and error distribution (lower) (scene identifier 239329911_R2A_AW__11-NOV-2023_100_063_GEOREF).

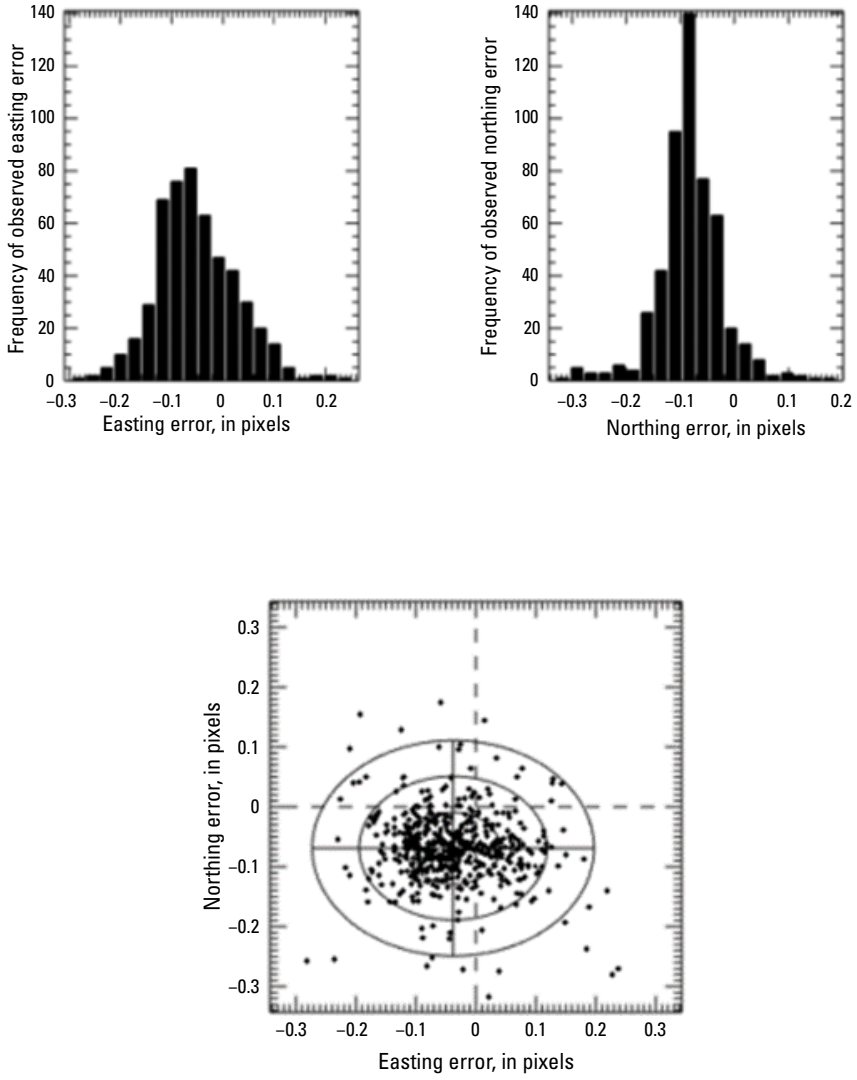

Figure 4. Band 3 (green) to band 5 (shortwave infrared) geometric error histogram (upper) and error distribution (lower) (scene identifier 239329911_R2A_AW__11-NOV-2023_100_063_GEOREF).

Exterior (Geometric Location Accuracy)

For this analysis, band 2 (green) of the AWiFS data was compared against the corresponding band from the Landsat 8 OLI image using the EROSSC software. Conjugate points in the reference and search images were identified automatically and refined using similarity measures such as normalized cross-correlation metrics. The mean error and RMSE results for three image pairs are listed in table 5 with results represented in meters at a 60-m GSD. Please note that the OLI (30-m GSD) and AWiFS (56-m GSD) images were resampled to 60 m. A geometric error map showing the directional shift and relative magnitude of the shift between AWiFS and Landsat 8 OLI is shown in figure 5. A corresponding error scatterplot and histograms for scene identifier 239329911_R2A_AW__11-NOV-2023_100_063_GEOREF are provided in figure 6.

Radiometric Performance

For this analysis, cloud-free regions of interest were analyzed within three AWiFS and Landsat 8 OLI scene pairs using the EROSSC software. Raw digital number-to-radiance conversion coefficients were obtained from the Indian Space Research Organisation. The scatterplots in figure 7 show the reference sensor on the x-axis and the comparison sensor on the y-axis. The linear regression represents Top of Atmosphere (TOA) reflectance relative to that of the reference sensor. Ideally, the slope should be near unity, and the offset should be near zero. For instance, if the slope is greater than unity, the comparison sensor is overestimating the TOA reflectance compared to the reference sensor.

TOA reflectance comparison results of the three scene pairs used for the analyses are listed in table 6. A band-by-band graphical comparison between AWiFS scene identifier 239329911_R2A_AW__11-NOV-2023_100_063_GEOREF and the corresponding Landsat 8 OLI band is shown in figure 7.

AWiFS radiometric quality is also assessed by comparing it with Radiometric Calibration Network (RadCalNet; Bouvet and others, 2019) coincident measurements. RadCalNet provides automated TOA reflectance measurements that are used to calibrate and validate optical satellite sensors. AWiFS was compared to measurements from the RadCalNet instrumentation and a coincident Landsat 9 OLI image over the Railroad Valley playa, Nevada, site. The AWiFS footprint over Railroad Valley playa is shown in figure 8, and the red box represents the 700-m x 700-m region of interest used to extract AWiFS and Landsat 9 OLI TOA reflectance.

The TOA reflectance comparison among AWiFS, RadCalNet, and Landsat 9 (Earth Resources Observation and Science Center, 2020) is shown in figure 9*A* and *B* on two dates: July 29, 2023 (239330721_R2A_AW__29-JUL-2023_252_045_GEOREF), and September 15, 2023 (239330711_R2A_AW__15-SEP-2023_252_045_GEOREF), respectively. For the radiometric comparison, RadCalNet hyperspectral TOA reflectance is used to simulate AWiFS TOA reflectance using the AWiFS relative spectral response. In figure 9*A* and *B*, blue symbols represent the TOA reflectance ratio between AWiFS and RadCalNet, whereas green symbols represent the TOA reflectance ratio between AWiFS and Landsat 9 OLI observations. For the September 15, 2023, comparison in figure 9*B*, AWiFS agrees with RadCalNet within 13 percent across all the bands, and the shortwave-infrared band has the best agreement (within 5 percent). AWiFS agrees with Landsat 9 OLI within 11 percent for the near-infrared and shortwave-infrared bands, but it is only within 14 percent and 16 percent for the red and green bands, respectively. For the July 29, 2023, comparison, figure 9*A* shows a better agreement with AWiFS being within 5 percent for RadCalNet and Landsat 9 OLI.

The AWiFS radiometric assessment was also completed by comparing the sensor with Landsats 8 and 9 OLI using pseudoinvariant calibration sites (PICS). Footprints of AWiFS, Landsat 9, and Hyperion (Folkman and others, 2001) over the Libya 1 PICS site in the Sahara Desert in Libya are shown in figure 10. The red box represents the region of interest used to compare AWiFS and Landsat 9 OLI TOA reflectance. The spectral difference between the two sensors is compensated for by calculating a spectral band adjustment factor (SBAF) for AWiFS using Hyperion hyperspectral data.

The comparisons between AWiFS and Landsat using the Libya 1 PICS site and the Algeria 5 PICS site (in the Grand Erg Occidental in Algeria) are shown in figure 11*A* and *B*. The mean TOA reflectance ratio between AWiFS and Landsats 8 and 9 OLI is shown in figure 11*A*. AWiFS agrees with Landsat within about 7 percent, and the best agreement was observed in the red and near-infrared bands. In figure 11*B*, the TOA reflectance ratio using the individual PICS sites is shown. The reflectance ratios between AWiFS and Landsats 8 and 9 for the Libya 1 site are more consistent than for the Algeria 5 site.

The results of the SBAF analyses are summarized in table 7. The SBAF should be interpreted such that a factor of 1 indicates a perfect alignment of spectral bands and calibration between Landsat and AWiFS.

Spatial Performance

For this analysis, edge spread and line spread functions were calculated using the automated methods that extract natural edges found in rural areas, and uniform surfaces were on either side of the edges. The resulting relative edge response, full width at half maximum, and modulation transfer function at Nyquist frequency (Oppenheim and others, 1997) analysis output values are listed in table 8. The area selected consists of farmland over Germany (scene identifier 239330611_R2A_AW__10-JUN-2023_026_032_GEOREF).

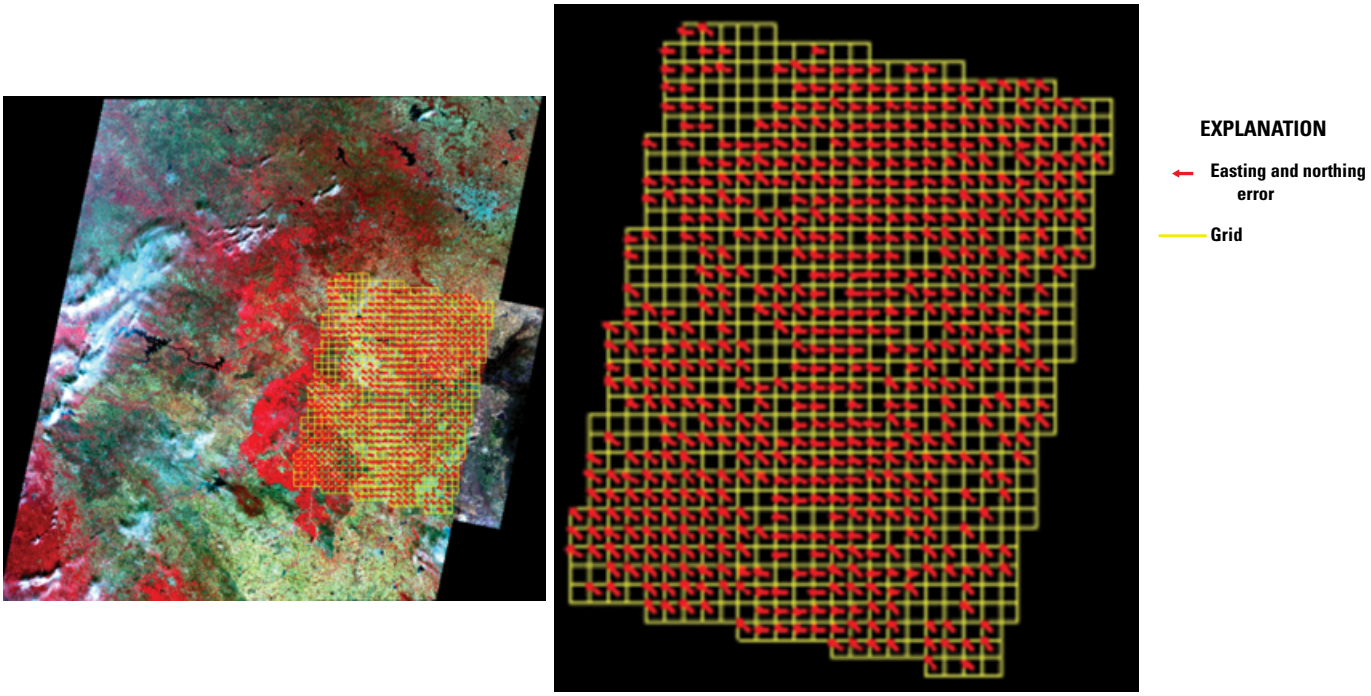

Figure 5. Geometric error comparison for Landsat 8 Operational Land Imager and Resourcesat-2A Advanced Wide Field Sensor (scene identifier 239329911_R2A_AW__11-NOV-2023_100_063_GEOREF).

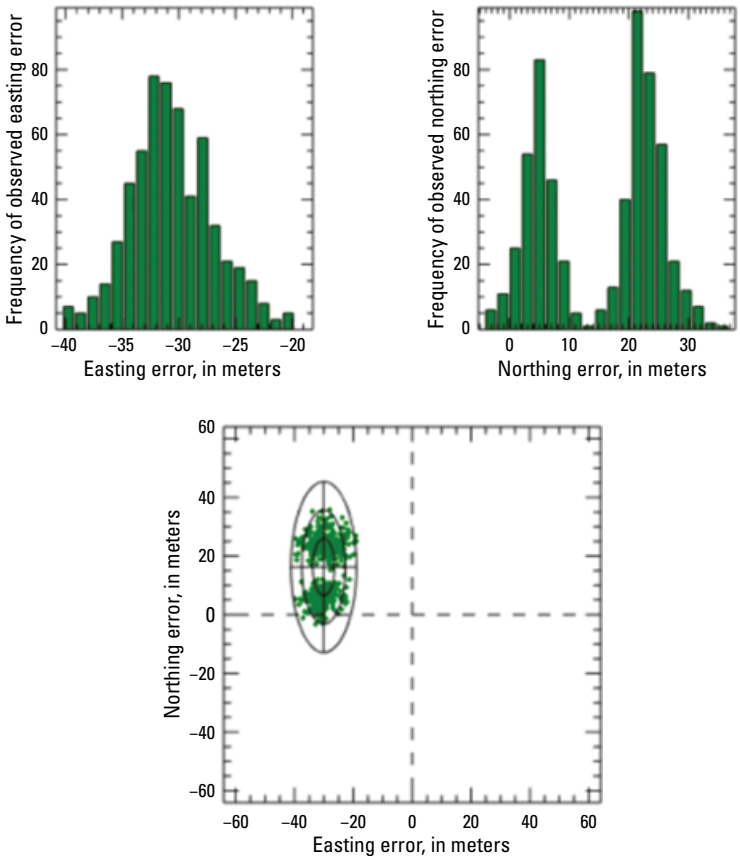

Figure 6. Geometric error histogram (upper) and error distribution (lower) (scene identifier 239329911_R2A_AW__11-NOV-2023_100_063_GEOREF).

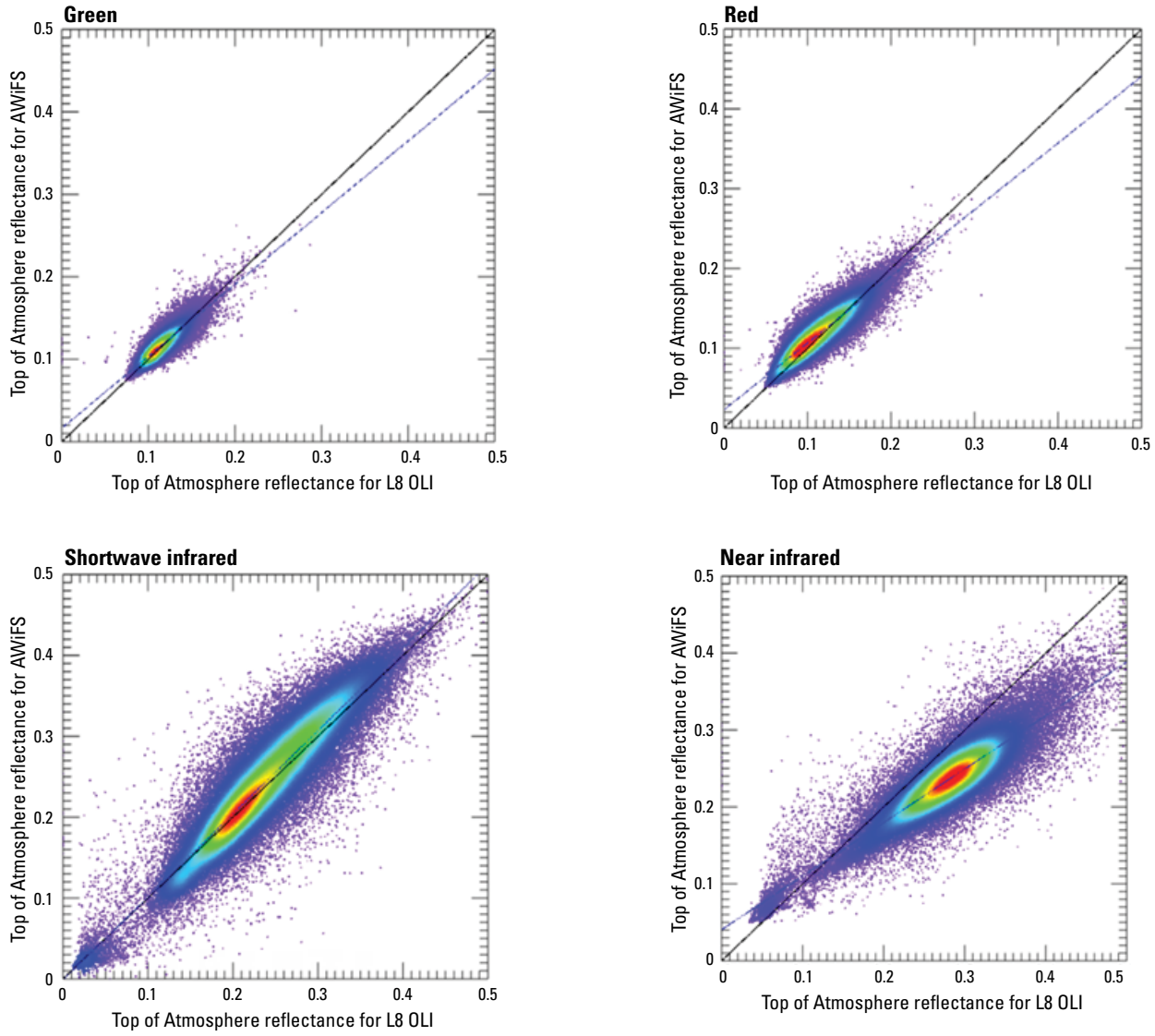

Figure 7. Graphs showing Top of Atmosphere reflectance comparison for Landsat 8 Operational Land Imager (L8 OLI; Earth Resources Observation and Science Center, 2020) and Resourcesat-2A Advanced Wide Field Sensor (AWiFS; Indian Space Research Organisation, 2023).

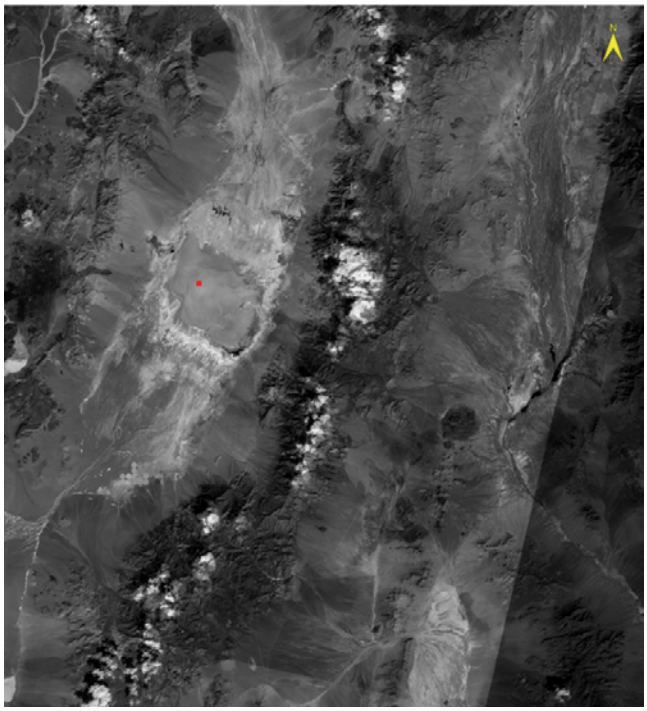

Figure 8. Image showing Advanced Wide Field Sensor (Indian Space Research Organisation, 2023) footprint over Railroad Valley playa, Nevada.

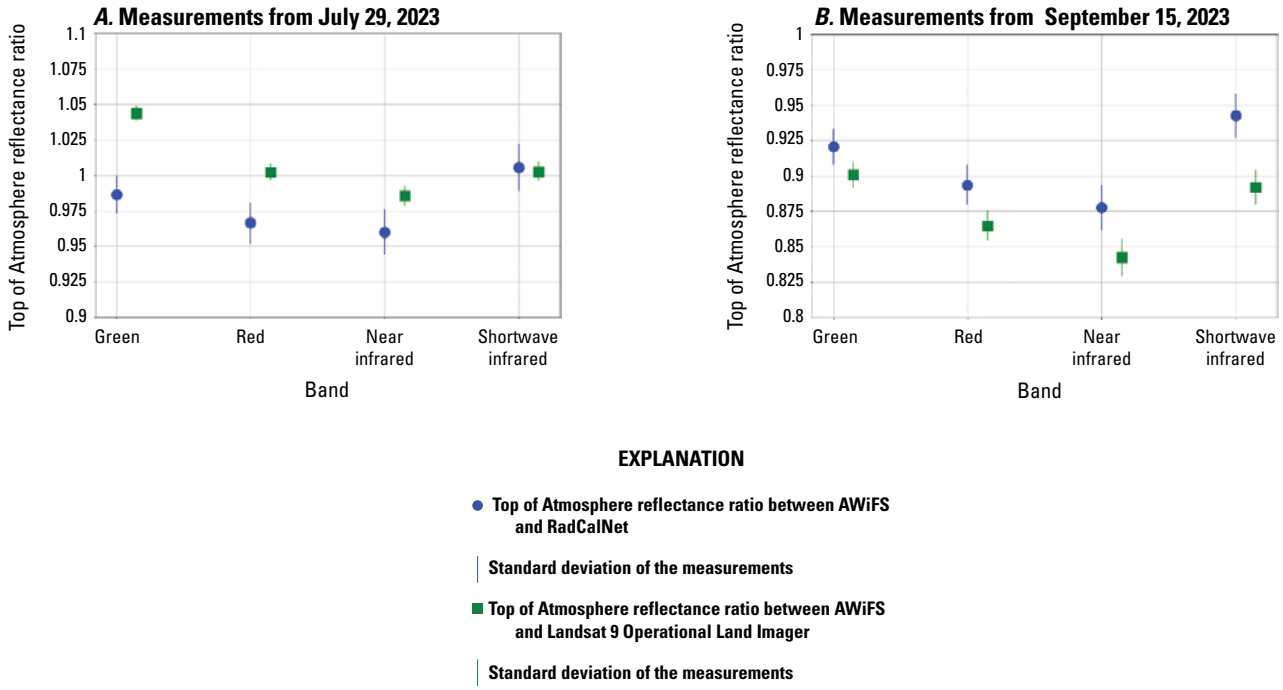

Figure 9. Graphs showing the Advanced Wide Field Sensor (AWiFS; Indian Space Research Organisation, 2023) comparison with Radiometric Calibration Network (RadCalNet; Bouvet and others, 2019) and Landsat 9 (Earth Resources Observation and Science Center, 2020) on (*A*) July 29, 2023, and (*B*) September 15, 2023.

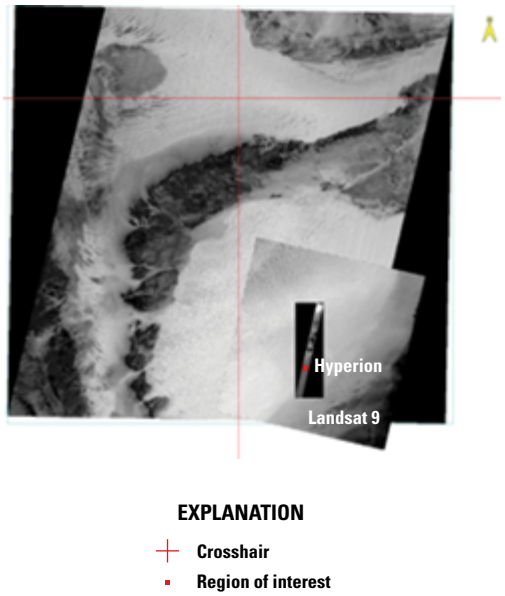

Figure 10. Images showing the Advanced Wide Field Sensor (AWiFS; Indian Space Research Organisation, 2023), Landsat 9 (Earth Resources Observation and Science Center, 2020), and Hyperion (Folkman and others, 2001) footprints over the Libya 1 site in the Sahara Desert in Libya.

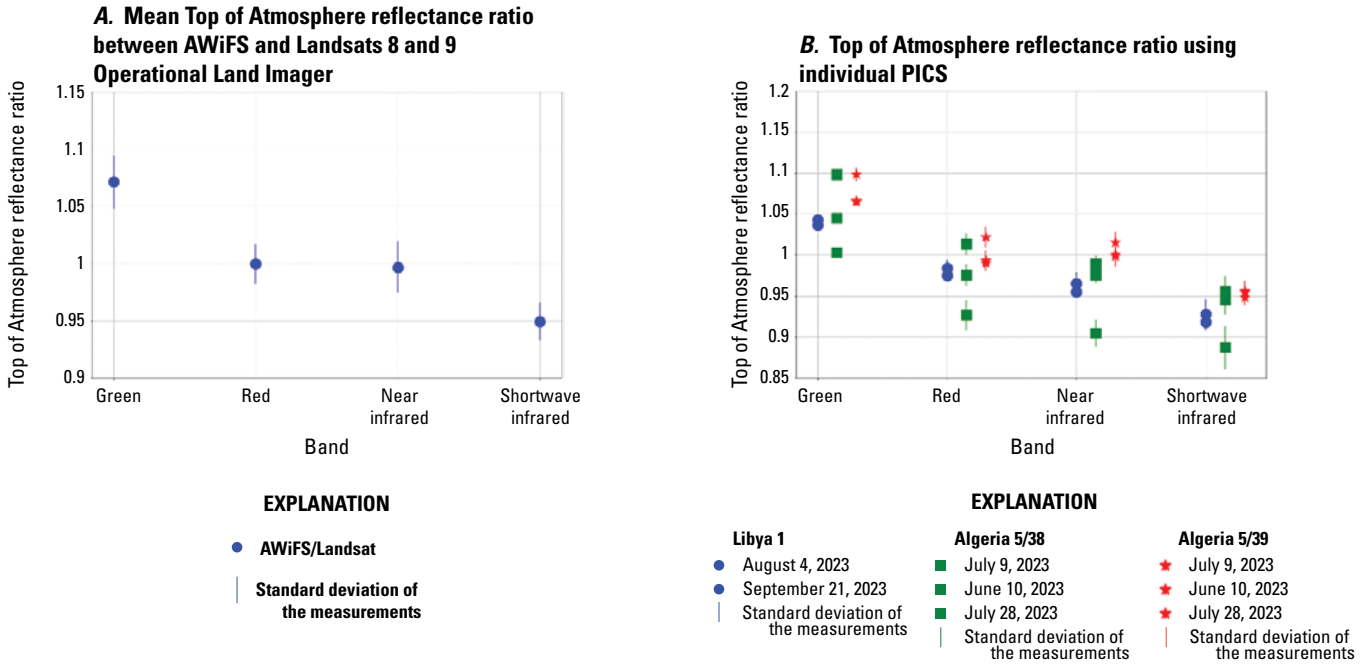

Figure 11. Graphs showing the Advanced Wide Field Sensor (AWiFS; Indian Space Research Organisation, 2023) comparison with Landsat (Earth Resources Observation and Science Center, 2020) using pseudoinvariant calibration sites (PICS) for (*A*) the Top of Atmosphere reflectance ratio between AWiFS and Landsats 8/9 Operational Land Imager and (*B*) the individual reflectance ratio from the Libya 1 and Algeria 5 sites. [The Libya 1 site is in the Sahara Desert in Libya; the Algeria 5 site is in the Grand Erg Occidental in Algeria]

Table 8. Spatial performance of Resourcesat-2A Advanced Wide Field Sensor (Indian Space Research Organisation, 2023).

[RER, relative edge response; FWHM, full width at half maximum; MTF, modulation transfer function; NIR, near infrared; SWIR, shortwave infrared]

Spatial analysis	RER	FWHM (pixels)	MTF at Nyquist
Band 2—green	0.601	1.429	0.174
Band 3—red	0.574	1.354	0.154
Band 4—NIR	0.559	1.547	0.148
Band 5—SWIR	0.541	1.639	0.108

Summary and Conclusions

This report summarizes the sensor performance of the Resourcesat-2A Advanced Wide Field Sensor (AWiFS) based on the U.S. Geological Survey Earth Resources Observation and Science Cal/Val Center of Excellence (ECCOE) system characterization process.

In summary, ECCOE has determined that this sensor provides an interior geometric performance with band-to-band mean offsets in the range of −1.10 meters (m; −0.020 pixel) to 3.67 m (0.066 pixel) in easting and −5.68 m (−0.101 pixel) to 10.38 m (0.185 pixel) in northing with root mean square error values in the range of 5.60 m (0.100 pixel) to 11.31 m (0.202 pixel) in easting and 3.00 m (0.054 pixel) to 13.52 m (0.241 pixel) in northing.

We have measured the mean exterior geometric error offset to be −25.29 m in easting and 16.22 m in northing with root mean square error values of 26.07 m in easting and 17.60 m in northing in comparison to the Landsat 8 Operational Land Imager sensor.

The measured radiometric performance was in the range of −0.002 to 0.029 in offset and 0.733 to 1.012 in slope, and the spatial performance was in the range of 1.354 to 1.639 pixels for full width at half maximum with a modulation transfer function at a Nyquist frequency in the range of 0.108 to 0.174.

In conclusion, the ECCOE team completed a standardized system characterization of the Resourcesat-2A AWiFS sensing system. Although the team followed characterization procedures that are standardized across the many sensors and sensing systems under evaluation, these procedures are customized to fit the individual sensor as was done with AWiFS. The team acquired the data, defined proper testing methodologies, carried out comparative tests against specific references, recorded measurements, completed data analyses, and quantified sensor performance accordingly. The team archived all data and measurements and documented the evaluation methods, which ensures that all data and measurements remain accessible so that the performance results can be reproduced if necessary.

The ECCOE project and associated Joint Agency Commercial Imagery Evaluation partners are always interested in reviewing sensor and remote sensing application assessments and would like to review and discuss information on similar data and product assessments and reviews. If you would like to discuss system characterization with either the U.S. Geological Survey ECCOE or Joint Agency Commercial Imagery Evaluation teams, please email us at eccoe@usgs.gov.

References Cited

Bouvet, M., Thome, K., Berthelot, B., Bialek, A., Czapla-Myers, J., Fox, N.P., Goryl, P., Henry, P., Ma, L., Marcq, S., Meygret, A., Wenny, B.N., and Woolliams, E.R., 2019, RadCalNet—A radiometric calibration network for Earth observing imagers operating in the visible to shortwave infrared spectral range: Remote Sensing (Basel), v. 11, no. 20, 24 p., accessed March 11, 2025, at https://doi.org/10.3390/rs11202401.

Cantrell, S.J., and Christopherson, J.B., 2024, Joint Agency Commercial Imagery Evaluation (JACIE) best practices for remote sensing system evaluation and reporting: U.S. Geological Survey Open-File Report 2024–1023, 26 p., accessed April 16, 2025, at https://doi.org/10.3133/ofr20241023.

Clauson, J., Cantrell, S., Vrabel, J., Oeding, J., Ranjitkar, B., Rusten, T., Ramaseri, S., and Casey, K., 2024, Earth observing sensing satellites online compendium: U.S. Geological Survey digital data, accessed March 7, 2025, at https://calval.cr.usgs.gov/apps/compendium.

Earth Resources Observation and Science Center, 2020, Landsat 8–9 Operational Land Imager/Thermal Infrared Sensor Level-1, Collection 2: U.S. Geological Survey digital data, accessed April 16, 2025, at https://doi.org/10.5066/P975CC9B.

Folkman, M.A., Pearlman, J., Liao, L.B., and Jarecke, P.J., 2001, EO-1/Hyperion hyperspectral imager design, development, characterization, and calibration: Hyperspectral Remote Sensing of the Land and Atmosphere, v. 4151, p. 40–51. [Also available at https://doi.org/10.1117/12.417022.]

Indian Space Research Organisation, 2023, Resourcesat-2A: Indian Space Research Organisation web page, accessed August 30, 2024, at https://www.antrix.co.in/.

Oppenheim, A.V., Willsky, A.S., and Nawab, S.H., 1997, Signals & systems (2d ed.): Upper Saddle River, N.J., Prentice Hall, 957 p.

U.S. Geological Survey, 2021a, EROS CalVal Center of Excellence (ECCOE): U.S. Geological Survey web page, accessed October 2024 at https://www.usgs.gov/calval.

U.S. Geological Survey, 2021b, EROS CalVal Center of Excellence (ECCOE)—JACIE: U.S. Geological Survey web page, accessed October 2024 at https://www.usgs.gov/calval/jacie.

U.S. Geological Survey, 2021c, Landsat missions—Glossary and acronyms: U.S. Geological Survey web page, accessed June 2021 at https://www.usgs.gov/core-science-systems/nli/landsat/glossary-and-acronyms.

For more information about this publication, contact:
Director, USGS Earth Resources Observation and Science Center
47914 252nd Street
Sioux Falls, SD 57198
605–594–6151

For additional information, visit: https://www.usgs.gov/centers/eros

Publishing support provided by the
Rolla Publishing Service Center

ISSN 2331-1258 (online)
https://doi.org/10.3133/ofr20211030V